Available online at www.sciencedirect.com
ScienceDirect
Journal of Asian Earth Sciences 30 (2007) 433–447
Journal of Asian Earth Sciences
www.elsevier.com/locate/jaes

Post-collisional Miocene adakitic volcanism in NW Iran: Geochemical and geodynamic implications

Ahmad Jahangiri

Department of Geology, University of Tabriz, 51664 Tabriz, Iran

Received 14 October 2005; received in revised form 15 November 2006; accepted 27 November 2006

Abstract

In NW Iran, about 30 subvolcanic porphyritic dacitic to rhyodacitic domes (1–5 km^2) are intruded into a variety of rock sequences from Permian to Early Miocene in age. These subvolcanic domes occur along the North Tabriz, North Misho and Darediz dextral faults in the northern part of the Urumieh-Dokhtar magmatic arc (UDMA) of Iran. The UDMA contains intrusive and extrusive rocks of Eocene-Quaternary age. Geochemical data indicate that the subalkalic dacitic to rhyodacitic rocks have an adakitic composition with $Na_2O/K_2O > 1$, high Sr (346–737 ppm), Mg# = 0.48 and low Y (10–20 ppm) and HREE. Fractionated REE patterns, $(Ce/Yb)_N$ = 9–76, absence of negative Eu anomaly, low content of Y, Nb, Ti, and high Sr/Y (20–58) and $(Ce/Yb)_N$ ratios suggest that the source was probably amphibole-eclogite or garnet-eclogite, possibly generated during subduction of the Neo-Tethyan oceanic slab beneath the Central Iran microplate. The adakitic volcanism was followed by eruption of alkaline magmas including ultrapotassic, shoshonitic, and lamprophyric volcanic rocks. Slab melting occurred after cessation of subduction, possibility from the detached slab. Transtensional tectonics accompanied by a locally extensional stress regime may account for magma genesis and ascent.

Keywords: Post-collision; Dacite; Adakite; Neo-Tethys; Iran

1. Introduction

The Tethyan orogenic collage formed from collision of dispersed fragments of Gondwana with Eurasia (Ricou, 1994; Sengör, 1984; Mohajjel et al., 2003). Within this context, three major tectonic elements with NW–SE trends are recognized in Iran due to collision of the Afro-Arabian continent and Iranian microcontinent. They include the Urumieh-Dokhtar magmatic arc (UDMA), the Sanandaj-Sirjan metamorphic zone and Zagros-Folded-Thrust belt (Fig. 1, Alavi, 1994; Mohajjel et al., 2003). The Urumieh-Dokhtar magmatic arc contains intrusive and extrusive rocks of Eocene-Quaternary age that forms a zone 50 km wide and 4 km thick (Berberian and Berberian, 1981) that extends from NW to SE in Iran. However, peak of magmatic activity is thought to be of Eocene age (e.g. Stöcklin, 1974; Farhoudi, 1978; Emami, 1981; Alavi, 2004). Geochemical studies indicate that the Urumieh-Dokhtar magmatic arc is generally composed of subduction-related calc-alkaline rocks (e.g. Förster et al., 1972; Jung et al., 1976; Berberian et al., 1982). Alkaline rocks also are reported locally by Amidi et al. (1984), Hassanzadeh (1993) and Moradian (1997). Amidi et al. (1984) proposed a rift model to interpret the genesis of Eocene magmatic rocks in the UDMA. Berberian and Berberian (1981) argued that the onset of alkaline volcanism, which followed the calc-alkaline volcanism (6-5 Ma) in NW Iran, was due to sinking of the final broken pieces of oceanic slab to a depth where alkaline melts were generated. Ghasemi and Talbot (2006) suggest that post-suturing magmatic activity along the Sanandaj-Sirjan zone and UDMA can be attributed to slab break-off.

Towards NW Iran and adjacent to the Anatolia plate and Armenia highland, the above-mentioned three zones become narrow and increase in geologic complexity and

E-mail address: A.Jahangiri@tabrizu.ac.ir

1367-9120/$ - see front matter © 2007 Elsevier Ltd. All rights reserved.
doi:10.1016/j.jseaes.2006.11.008

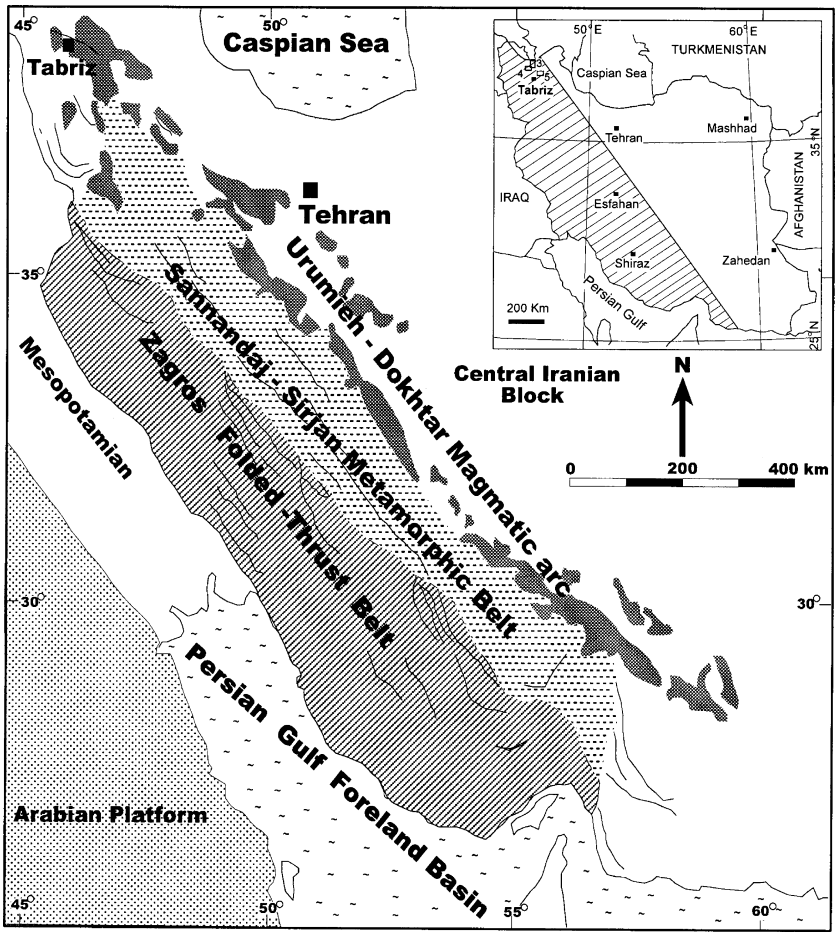

Fig. 1. Three main tectonic units of the Zagros orogenic belt (after Alavi, 1994; Mohajjel et al., 2003). Studied area is shown by the index map as boxes 3, 4 and 5.

magmatic activity from calc-alkaline, alkaline to peralkaline including those of shoshonitic affinity. The diversity of magmatic types from calc-alkaline to alkaline, including high-potassic volcanic rocks, indicate NW Iran to represent classical areas of young volcanism. The most intense eruptions were during the late collisional stage, which led to the formation of great volcanoes like Sabalan, Sahand, Keyamaki-Daghi and other volcanoes in NW Iran.

The great diversity of Neogene to Quaternary magmatic rocks, from dacitic to rhyodacitic subvolcanic domes and extending for more than 100 km, are of interest due to their specific conditions of formation and spatial and temporal relation with other magmatic rocks. The dacitic volcanism of late Miocene in NW Iran was followed by shoshonitic and alkaline volcanism (Ahmadzadeh, 2002). The temporal and spatial relationship of dacitic calc-alkaline magmatism with alkaline magmatism is also reported from different areas of Gondwana fragments and Eurasia plate collision zone (e.g. Pe-Piper and Piper, 1994; Seghedi et al., 2004; Chung et al., 2005).

The aims of this paper are (1) to present the main geochemical characteristics of the dacitic to rhyodacitic magmatism in NW Iran, (2) to suggest the conditions of their genesis, and (3) to discuss the geodynamic environment in which they could have formed.

2. Regional setting

The investigated areas are situated at the northern side of the North-Tabriz dextral fault and at the north of Tabriz City (Figs. 1–5). In this area, numerous ($n \sim 30$) subvolcanic domes with NW–SE trends are intruded into different volcanic, volcano-sedimentary and sedimentary rocks. In the northern part of the studied area, SE of Jolfa City and Aras River, subvolcanic domes are intruded into Permo-Triassic limestones, Cretaceous-Paleocene flysch and Eocene limestone and sandstones (Fig. 3). The subvolcanic domes, ranging in outcrop area from 1 to 5 km^2. The Keyamaki-Daghi dome riser 3347 meters above sea level and is highest feature in this area. To the west and east of Marand City (Fig. 4) the subvolcanic domes intruded into the Eocene volcanic, volcaniclastic rocks and sedimentary sequence forming part of the Upper Red Formation. The Eocene volcanic and volcaniclastic rocks consist of basalt, andesitic-basalt, brecciated volcaniclastic rocks and green tuffs (Fig. 4). On the southern part of the studied

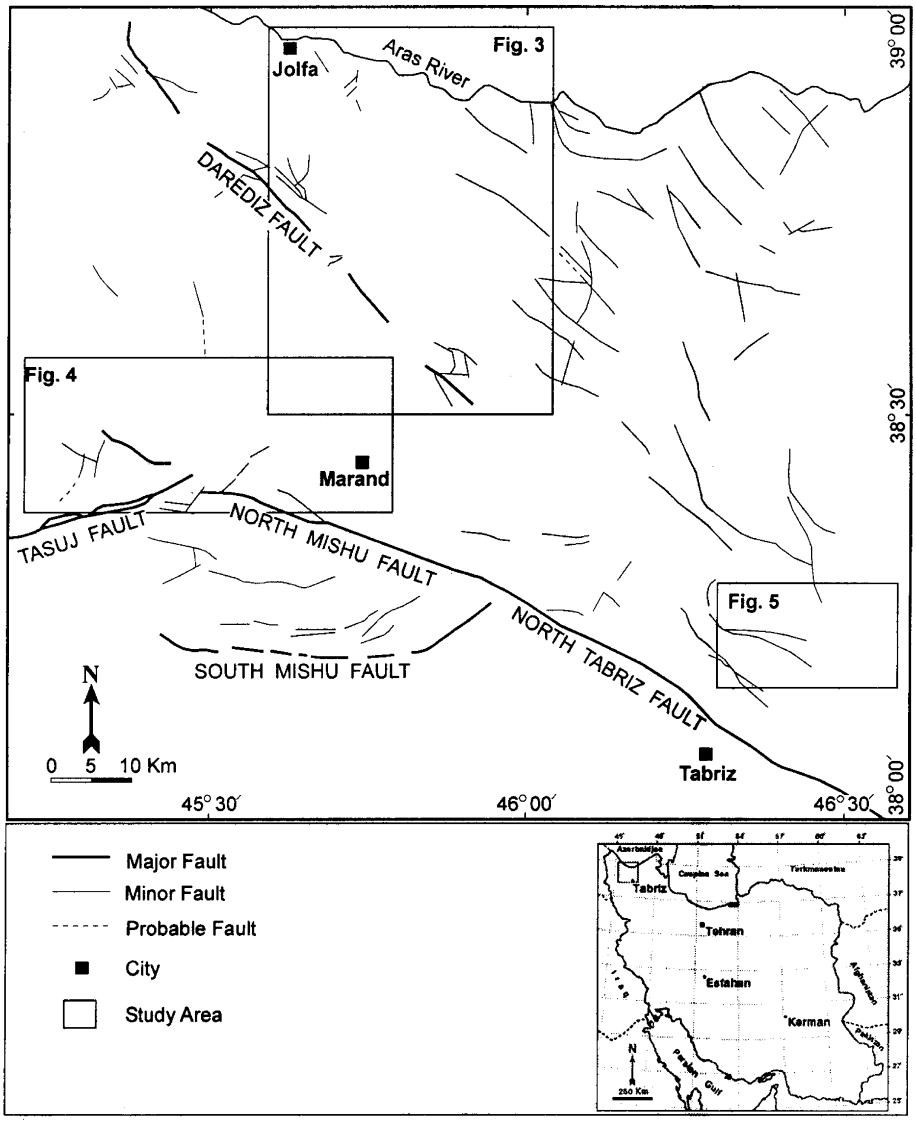

Fig. 2. Tectonic map of the studied area, showing dacitic to rhyodacitic domes bounded to the main dextral faults.

area in the Nahand region (Fig. 5), the volcanic domes are intruded into the Upper Red Formation sedimentary sequences of Miocene age. The Upper Red Formation covers an extensive area in Central and NW Iran. This formation is composed of conglomerate, sandstone, red shales and marls with evaporates (Stöcklin, 1972; Asadian, 1993; Karimzadeh Somarin, 2004). The age of emplacement of the subvolcanic domes has not been determined by geochronological dating, but based on stratigraphical studies, these domes are Middle to Late Miocene in age. This stratigraphical age is consistent with dating of rhyolitic domes by Karapetian et al. (2001), which yield ages of 10–17 Ma based on whole rock Rb/Sr and K/Ar dating methods for early stage post-collision rhyolitic domes in the Armenia Highland. Field studies and remote sensing investigations indicate that these domes were emplaced along normal faults and fractures that developed in conjunction with the North-Tabriz, North Misho (Sadeghzadeh, 2004) and Darehdiz dextral faults (Fig. 2). Strike-slip tectonics accompanied by a transtensional régime may also account for generation of some of the magmatic suites (e.g., adakite, calc-alkaline, alkaline and shoshonite) in this region.

3. Petrographic features

The porphyritic volcanic rocks consist of intermediate to felsic suites whose composition varies from hornblende-andesite, dacite to rhyodacite and rhyolite. Dacitic rocks are dominant and show porphyritic texture with phenocrysts of plagioclase and hornblende. Plagioclase is the ubiquitous phenocryst (25–35 vol%) and contains inclusions of apatite, magnetite, amphibole and zircon. Andesites and dacites contain large plagioclase crystals (3–5 mm) that usually exhibit sieve textures and well defined zoning marked by concentric zones rich in/or devoid of glass and opaque inclusions. In some samples, plagioclase phenocrysts are mantled by a rim devoid of inclusions, whereas

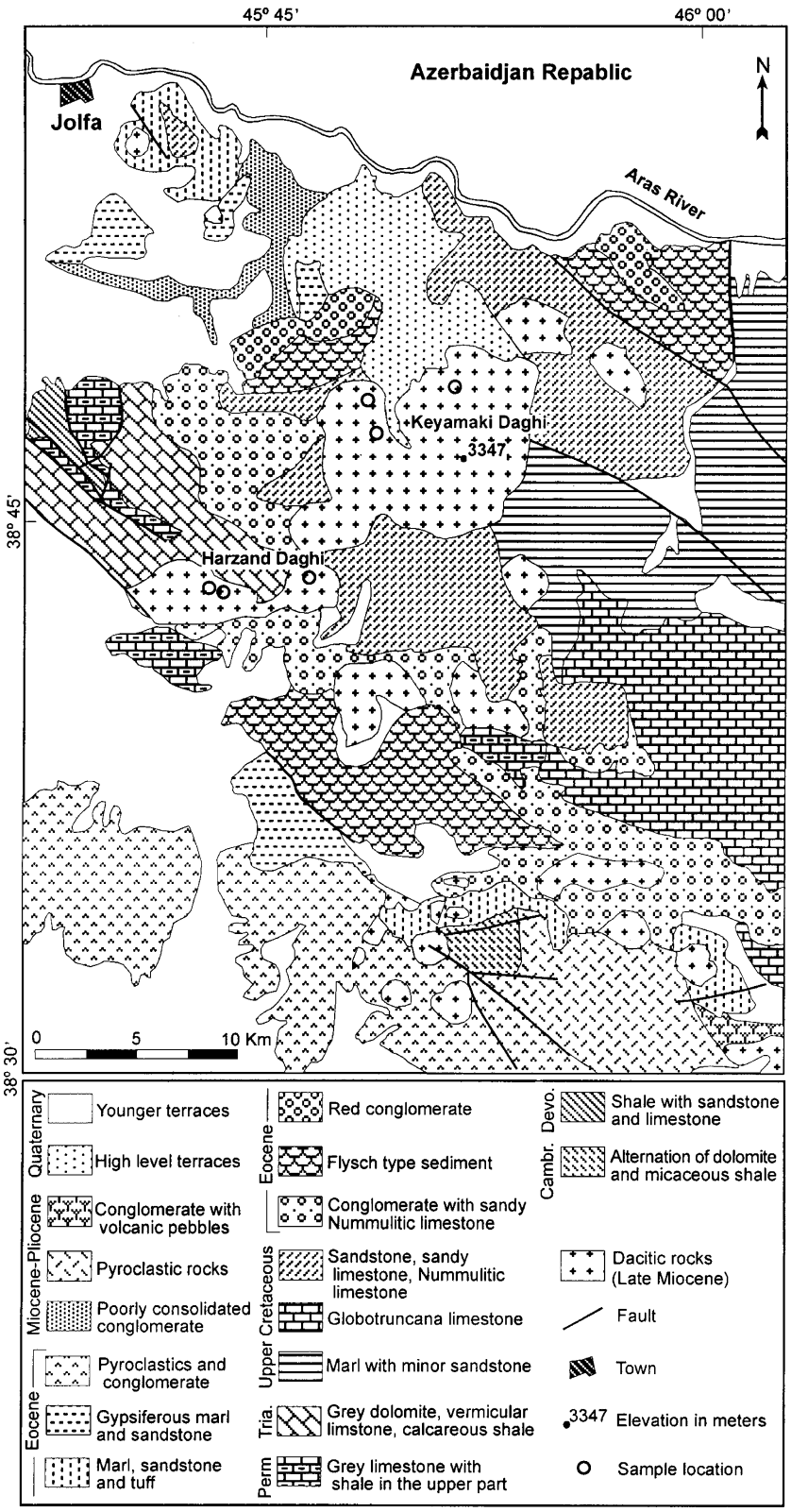

Fig. 3. Geological map of the Jolfa area. (Simplified from the geological map of 1:250,000 Tabriz).

the core is rich in inclusions. These samples are rich in K_2O (see below).

Hornblende occurs as the main ferromagnesian phenocryst (up to 3 mm) in andesite and dacite and varies from green to brown in color. It contains inclusions of apatite, zircon and titanomagnetite. Oxyhornblende phenocrysts occur in rhyodacitic samples of the Nahand area. In some samples, accumulation of hornblende led to formation of

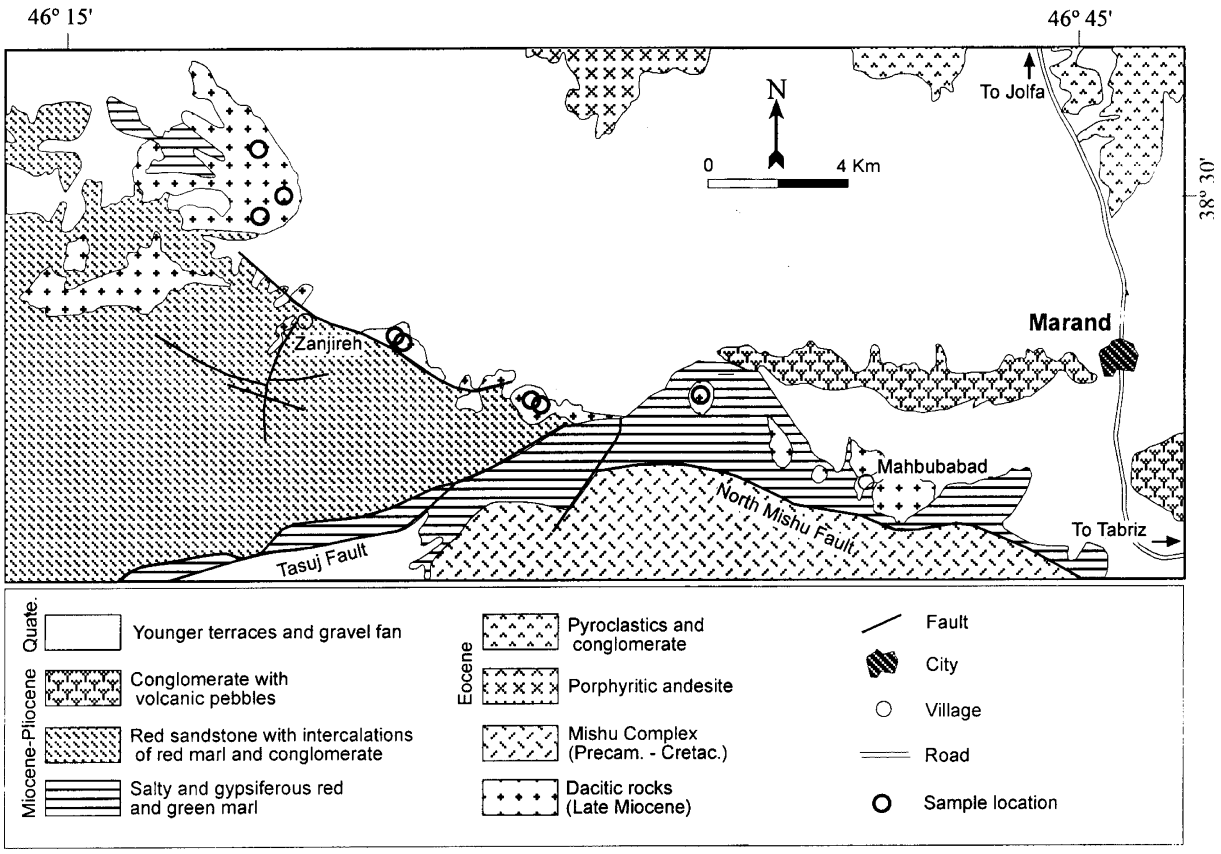

Fig. 4. Geological map of the Marand region. (Simplified from the geological map of 1:250,000 Tabriz).

glomeroporphyric texture. The groundmass is composed of plagioclase and hornblende as the main minerals, with apatite, biotite, quartz and iron oxides as accessory minerals. Rhyodacites and rhyolites have embayed plagioclase, sanidine, augite, and biotite interpreted as a result of resorbtion in a groundmass of plagioclase, quartz and iron oxide.

4. Geochemical characteristics

4.1. Analytical methods

About 150 samples of the dacitic rocks were collected from different domes. In order to correctly characterize their chemical compositions, 21 least-altered samples were chosen for major, trace and rare-earth-elements (REE) analysis. Samples for whole rock analysis were crushed and powdered in agate ball-mills. Major and trace elements were determined on fused glass and pressed powder discs, using a Bruker S4 X-ray fluorescence spectrometer (XRF) at Tabriz University. Inductively Coupled Plasma-Mass Spectrometry (ICP-MS) and INNA were employed for REE and trace element analysis of 8-selected samples at Actlabs laboratories (Canada). Representative chemical analysis for major, trace and rare earth elements are presented in Table 1. The detection limit for major elements is 0.01 wt% except for Ti and P, which is 0.005 wt%. The detection limits for trace elements are shown in Table 1 in brackets.

4.2. Analytical results

The SiO_2 content of samples vary from 65 to 73 wt%. The chemical compositions of the rocks are plotted on the total alkalis vs. silica (TAS) diagram (Fig. 6) of Le Maitre et al. (1989). The samples plot in the dacite and rhyolite field of this diagram. Using Zr/TiO_2 vs. SiO_2 diagram of Winchester and Floyd (1977) for classification of volcanic rocks, the studied samples plot in the fields of dacite and rhyodacite (Fig. 7). These rocks are metaluminous with $Al_2O_3/(CaO + Na_2O + K_2O)$ ratios of 0.75–1.05.

Using SiO_2 as a fractionation index, the samples display chemical variations and clear trends on Harker diagrams (Fig. 8). On variation diagrams, Fe_2O_3, MgO, TiO_2, CaO and P_2O_5 display negative correlations suggesting that these volcanic rocks experienced fractionation of apatite, hornblende, titanomagnetite, and plagioclase. Among the trace elements, Nb, Zr, and Y exhibit a negative correlation with SiO_2 and Sr, Ba, K_2O display scattered trends.

The Na_2O/K_2O ratios vary from 1.01 to 2.95, except for samples from west of Marand which have ratios less than 1 (samples V1, V5, and V6). Most of the samples are plot in

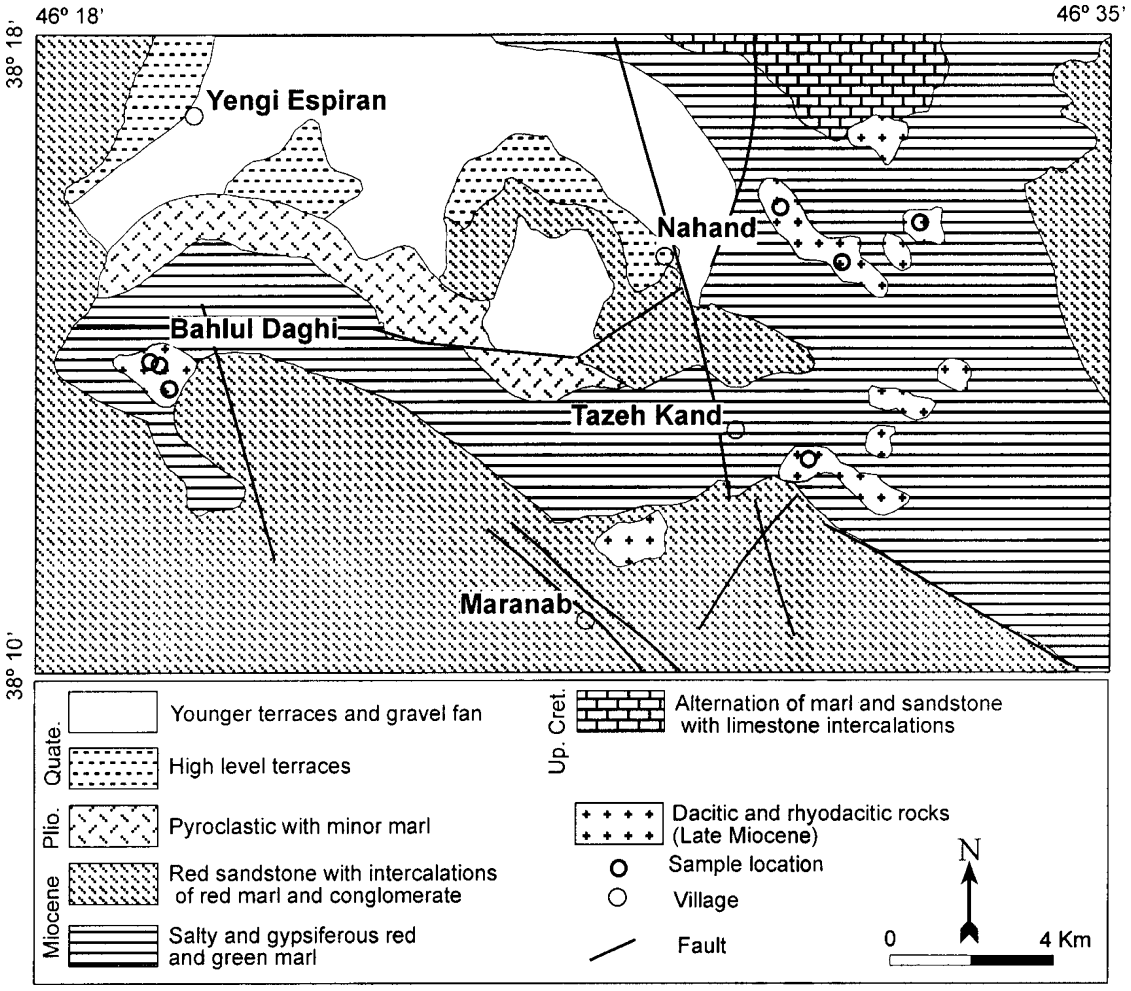

Fig. 5. Geological map of the Nahand region.

the medium-potassium field on the diagram of K_2O vs. SiO_2 (Fig. 9). In the AFM diagram of Irvine and Baragar (1971) and Y vs. Zr diagram (MacLean and Barrett, 1993), they plot in the calc-alkaline field (Fig. 10). The Mg# [MgO/(MgO + FeO)] of the samples ranges from 0.37 to 0.62, and contain high concentration of Sr (346–737 ppm) and low contents of Y and Rb. With regard to high Na_2O/K_2O ratios, the high contents of Sr, Mg# (mean 0.48) and low concentrations of Rb and Y indicate geochemical characteristics different from typical volcanic rocks. In the Y vs. Sr/Y diagram, most of the samples plot in the field of adakite relative to typical arc-related calc-alkaline rocks defined by Defant and Drummond (1990). A few samples plot near the intersection of the adakitic and calc-alkalic arc fields (Fig. 11).

Fig. 12 shows a spiderdiagram plot for representative samples from different domes normalized to primitive mantle composition (McDonough et al., 1992). All of the samples exhibit typical subduction-related signatures; they are enriched in large ion lithophile elements such as K, Rb and Ba and light REE relative to HFSE and HREE and negative Nb anomalies. They show significant positive anomalies for Sr, indicative of either the absence of plagioclase fractionation or retention of plagioclase in the residue. The adakites exhibit Sr enrichment, in contrast to non-adakitic dacites and rhyodacites which show negative anomalies in spiderdiagrams.

Fig. 13 displays the incompatible element patterns of representative samples normalized to average N-MORB of Pearce and Parkinson (1993). LILE and LREE enrichment can result from low degree partial melting of a MORB source. Decoupling of Zr and Ti with similar bulk Kd's and greater depletion of Ti has been interpreted to reflect a residual phase in the source that fractionated Ti (Pearce and Parkinson, 1993) or Ti-bearing phases (Reagan and Gill, 1989). The strong depletion of Y and Yb corresponds to the presence of restite garnet in the eclogitic source. The representative samples display steeply dipping REE patterns $(Ce/Yb)_N = 9–76$ with weak positive Eu anomalies (Fig. 14). Less fractionated sample (V-4) belongs to the Valdian dome. Petrographical studies and major element data reveal that this dome has greater crustal contamination. Nevertheless, there are no cross-cutting REE patterns, suggesting that the studied magmatic suites are possibly related to and most likely derived from, the same initial melt.

Table 1
Major and trace element contents of reprsentative dacitic and rhyodacitic samples of NW Iran

Sample	Region																				
	Nahand							Jolfa						Marand							
	Bh-1	Bh-2	Bh-3	Bh-4	ST-2	ST-3	ST-5	H-1	H-2	H-3	KH-1	KH-2	KH-5	GH-1	GKH-1	GKH-2	GKH-4	V-1	V-4	V-5	V-6
SiO_2	71.12	73.21	72.73	71.07	68.94	70.81	71.08	70.99	71.33	67.53	68.04	67.24	67.39	70.33	66.46	66.81	67.11	66.76	65.73	65.69	65.44
TiO_2	0.243	0.226	0.244	0.244	0.432	0.413	0.419	0.143	0.333	0.408	0.435	0.435	0.431	0.234	0.682	0.351	0.674	0.62	0.596	0.599	0.606
Al_2O_3	15	14.12	14.43	14.43	14.2	13.93	13.87	14.15	14.06	15.1	14.63	15.01	14.89	14.13	14.5	15.19	14.53	14.26	15.41	13.63	14.5
$Fe_2O_3^*$	1.1	1.01	1.29	1.42	3.01	2.89	2.92	2.46	2.65	3.16	3.3	3.29	3.43	2.72	3.92	3.7	3.81	4.07	4.13	4.45	4.17
MnO	0.01	0.01	0.01	0.01	0.05	0.04	0.04	0.04	0.06	0.06	0.05	0.06	0.06	0.02	0.07	0.06	0.06	0.10	0.10	0.11	0.12
MgO	0.95	0.88	0.7	0.84	1.09	1.13	1.01	1.59	1.69	2.42	2.45	2.32	2.47	1.46	1.38	1.16	1.3	1.33	1.3	2.19	1.55
CaO	2.73	2.39	2.88	2.85	5.12	4.84	4.44	3.14	3.17	4.2	4.08	4.41	4.14	2.93	4.54	4.18	4.37	4.66	4.64	3.48	4.55
Na_2O	4.69	4.76	4.29	3.3	3.76	3.48	3.47	4.24	3.86	3.52	3.34	3.74	3.68	5.21	4	3.96	4.08	2.97	3.57	3.37	2.75
K_2O	2.83	2.33	2.5	3.5	2.15	1.7	1.81	2.25	2.25	2.49	2.41	2.45	2.57	1.77	3.28	3.46	3.3	3.37	3.54	4.58	3.83
P_2O_5	0.1	0.11	0.113	0.147	0.179	0.174	0.168	0.143	0.142	0.263	0.231	0.235	0.268	0.23	0.338	0.351	0.334	0.239	0.235	0.377	0.227
LOI	0.45	0.74	0.22	0.36	0.78	0.5	0.42	0.47	0.26	0.75	0.88	0.64	0.44	1.35	0.54	0.13	0.37	1.33	0.62	0.97	1.82
Total	99.23	99.78	99.40	98.17	99.71	99.91	99.65	99.62	99.81	99.90	99.85	99.83	99.77	100.38	99.71	99.35	99.94	99.71	99.87	99.45	99.56
Cl	137	206	165	139	48	60	65	145	139	3021	280	205	282	134	39	39	35	57	54	392	75
Na_2O/K_2O	1.66	2.04	1.72	0.94	1.75	2.05	1.92	1.88	1.72	1.41	1.39	1.53	1.43	2.94	1.22	1.14	1.24	0.88	1.01	0.74	0.72
Mg #	0.46	0.47	0.45	0.37	0.44	0.46	0.43	0.56	0.57	0.62	0.62	0.57	0.61	0.52	0.42	0.39	0.41	0.41	0.49	0.5	0.45
Ba (1)	860	733	749	1138	608	534	532	600	699	705	695	744	740	472	795	742	764	958	886	984	953
Rb (2)	35	33	47	55	42	39	40	61	75	77	77	69	73	46	94	94	92	95	93	119	101
Sr (2)	533	542	512	516	686	686	694	498	523	602	584	610	568	524	737	719	737	590	590	397	555
Y (1)	10	10	11	12	12	12	12	13	13	14	13	14	14	12	16	17	18	20	19	20	19.3
Zr (1)	122	123	121	105	113	115	111	116	112	119	114	130	115	105	217	203	214	183	198	188	199
Nb (0.2)	9	9	6	6	12	4	4	5	12	11	9	13	12	6	15	18	19	9	16	12	15
Th (0.1)	7	4	2	9	7	9	9	5	12	7	3	8	8	2	31	26	23	8	16	16	11
Pb (5)	18	3	8	11	9	16	9	15	8	18	17	4	7	9	12	21	21	23	24	26	15
Ga (1)	14	13	18	16	14	15	10	13	16	16	19	20	11	16	12	17	22	15	16		17
Zn (1)	34	26	45	25	48	51	51	37	45	38	36	47	42	28	55	50	53	44	87	80	53
Cu (1)	1	1	1	1	8	8	4	2	15	11	6	8	2	1	25	16	19	12	1	1	1
Ni (1)	7	3	4	8	14	13	15	19	20	37	31	32	25	1	46	36	42	9	10	12	4
V (1)	30	28	291	27	40	43	43	42	43	49	47	49	49	27	68	57	63	72	64	68	63
Cr (0.5)	1	1	1	1	8	9	8	9	9	15	15	18	18	1	38	39	42	5	1	6	1
Co (0.1)	4	5	7	2	3	9	7	6	6	4	8	6	6	3	13	9	6	7		10	3
U (0.1)	1	2	1	1	1	5	5	1	4	1	1	2	1	1	5	4	9	3	3	8	1
Ti	1456	1354	1462	1462	2588	2474	2510	1420	1995	2444	2606	2606	2582	1252	4085	2432	4037	3714	3570	3588	3630
P	436	480	493	641	780	759	732	623	619	1147	1007	624	1168	558	1474	1530	1456	1042	1025	1644	990
Rb/Sr	0.07	0.06	0.09	0.11	0.06	0.06	0.06	0.12	0.14	0.13	0.13	0.11	0.13	0.09	0.13	0.13	0.12	0.16	0.16	0.30	0.18
Sr/Y	53.30	54.20	46.55	43.00	57.17	57.17	57.83	38.31	40.23	43.00	44.92	43.57	40.57	43.67	46.06	42.29	40.94	29.50	31.05	19.85	28.76
Rb/Zr	0.29	0.27	0.39	0.52	0.37	0.34	0.36	0.53	0.67	0.65	0.68	0.53	0.63	0.44	0.43	0.46	0.43	0.52	0.47	0.63	0.51
La (0.05)	15.4	17.8	22	21.3	9	36.2	33.3	27.3	11	26.4	9	6	35	7	18	45	6.34	33	49.3	10	28
Ce (0.05)	19	21.4	23.3	25.2	17	44.3	40.6	35	21	34.7	22	22	108	14	58	123	9.69	49	65.5	31	96
Pr (0.01)	2.18		2.5			4.9	4.56	4.21		4.23							1.42		7.94		
Nd (0.05)	8.26		9.18			19.6	18.2	15.1		15.5							7.69		25.9		
Sm (0.01)	1.13		1.27			2.35	2.26	2.45		2.82							1.08		5.61		
Eu (0.05)	0.55		0.62			0.85	0.82	0.84		1							0.43		1.68		
Gd (0.01)	0.84		0.88			1.67	1.67	1.57		1.66							1.03		3.55		
Tb (0.01)	0.12		0.13			0.27	0.27	0.24		0.27							0.2		0.6		

(*continued on next page*)

Table 1 (*continued*)

Sample	Region																
	Nahand						Jolfa				Marand						
	Bh-1	Bh-2	Bh-3	Bh-4	ST-2	ST-3	ST-5	H-1	H-2	H-3	KH-1	KH-2	KH-5	GH-1	GKH-1	GKH-2	GKH-4	V-1	V-4	V-5	V-6
Dy (0.01)	0.72		0.68			1.44	1.49	1.36		1.48							1.19		3.29		
Ho (0.01)	0.11		0.1			0.26	0.27	0.19		0.24							0.22		0.57		
Er (0.01)	0.3		0.26			0.64	0.67	0.5		0.61							0.62		1.57		
Tm (0.05)	0.08		0.08			0.1	0.1	0.08		0.09							0.1		0.24		
Yb (0.05)	0.22		0.19			0.14	0.44	0.46		0.53							0.25		1.25		
Lu (0.01)	0.04		0.04			0.1	0.09	0.06		0.06							0.1		0.22		
∑REE	48.95		61.23			112.82	104.74	89.36		89.59							30.36		167.22		
$(Ce/Yb)_N$	20.88		29.6			76.5	22.31	18.39		15.83							9.37		11.55		

$Fe_2O_3^*$ as total Fe_2O_3. Major elements in wt%, trace elements and REE in ppm.

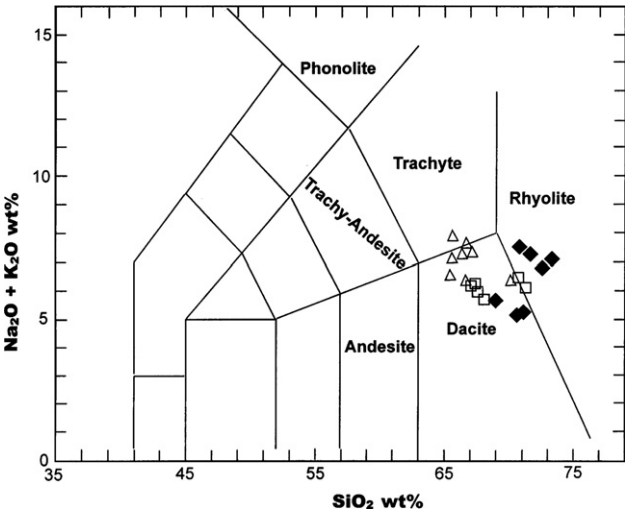

Fig. 6. Classification of volcanic rocks (Le Maitre et al., 1989). Composition of studied samples ranges from dacite to rhyolite.

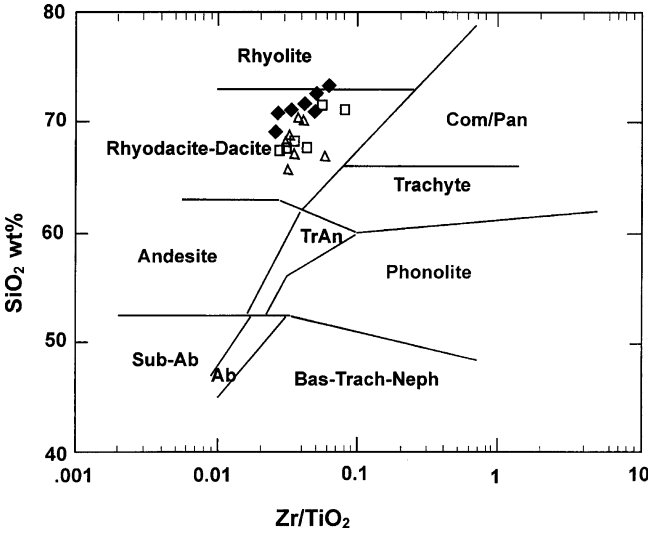

Fig. 7. Classification of volcanic rocks by Zr/TiO_2 vs. SiO_2 (Winchester and Floyd, 1977). Studied sample compositions range from dacite-rhyodacite to rhyolite.

5. Discussion

Geochemically, it appears that subduction related components played a controlling role in the genesis of the dacitic magmas in NW Iran. Enrichment of LILE and depletion of HFSE (Nb and Ti) and HREE are characteristic of subduction zone magmatism (Wilson, 1989). On the other hand, the high ratios of Na_2O/K_2O, high Sr, Mg# and Sr/Y ratios suggest an adakitic character for subduction-related magmatism (Defant and Drummond, 1990). The origin of adakites has been attributed to partial melting of either subducted oceanic crust converted to eclogite and garnet amphibolite (Kay, 1978; Defant

and Drummond, 1990; Drummond and Defant, 1990; Martin, 1993, 1999) or underplating of basaltic magmas under thick continental crust (Atherton and Petford, 1993; Petford and Atherton, 1996). The strongly fractionated REE pattern and depletions HREE and Y in adakites are possibly due to the presence of garnet ± amphibole in the melt residue. Their high Sr and low Nb, Ta and Ti contents are thought to be due to the absence of plagioclase and presence of Fe–Ti oxides in the residue (Martin, 1999). While geochemical data for igneous rocks compiled by Defant and Drummond (1990) indicate a relationship between subducted oceanic crust and adakite genesis, adakite occurrences in different tectonic environments led Maury et al. (1996) to propose that slab melting, even of old oceanic crust, is also possible during (1) the initiation of subduction (Sajona et al., 1993, 1994), (2) fast and oblique subduction (Kay, 1978; Peacock et al., 1994) and (3) termination of subduction (Prouteau et al., 1996; Sajona et al., 2000).

The high Mg and Cr content of most adakites are not consistent with the low concentration of these elements in experimentally produced melts of amphibolite or eclogite (Rapp et al., 1991; Sen and Dunn, 1995). Sen and Dunn (1994) and Yogodzinski et al. (1995) attributed this enrichment to interaction of adakitic magma with the mantle during ascent. Experimental work by Rapp et al. (1999) show

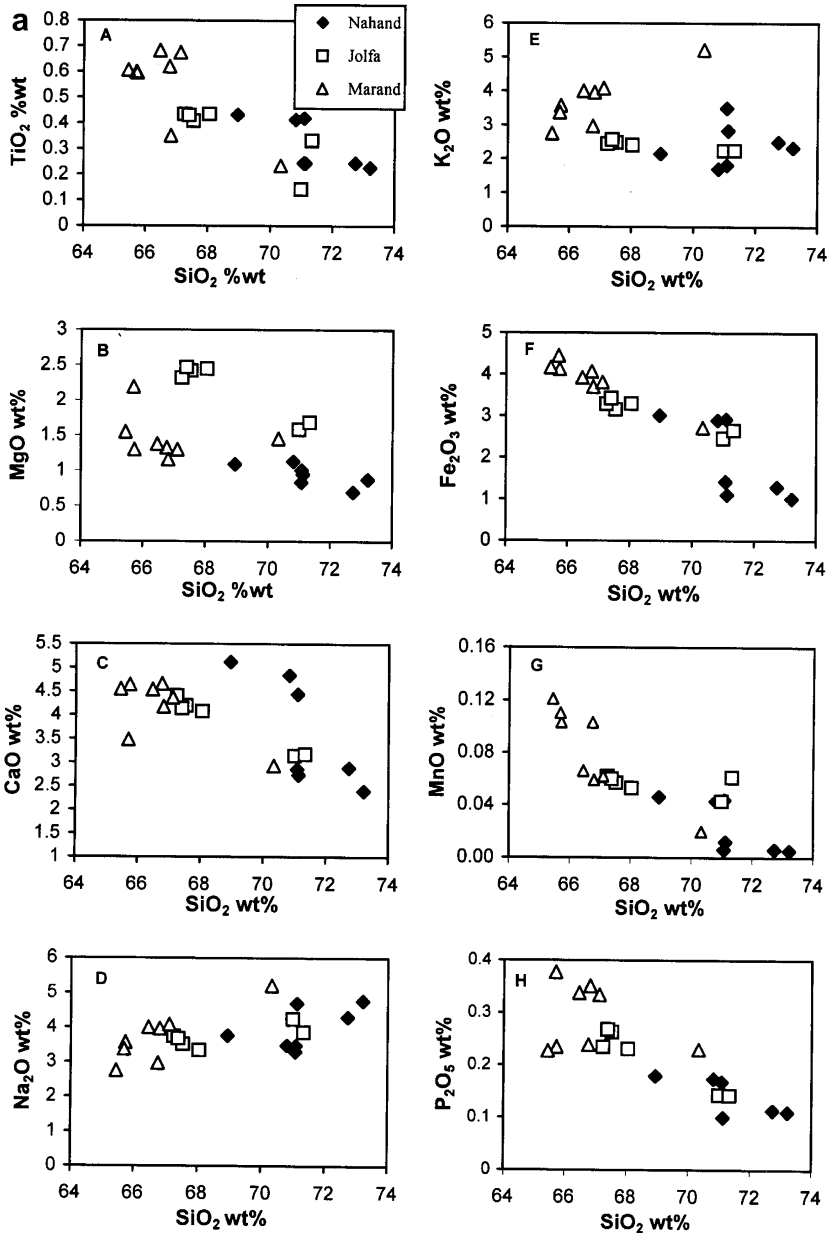

Fig. 8. Variation diagrams for major and trace elements of dacitic and rhyodacitic rocks of NW Iran. Major and trace elements are in wt% and ppm, respectively. Fe_2O_3 as $Fe_2O_{3\ total}$.

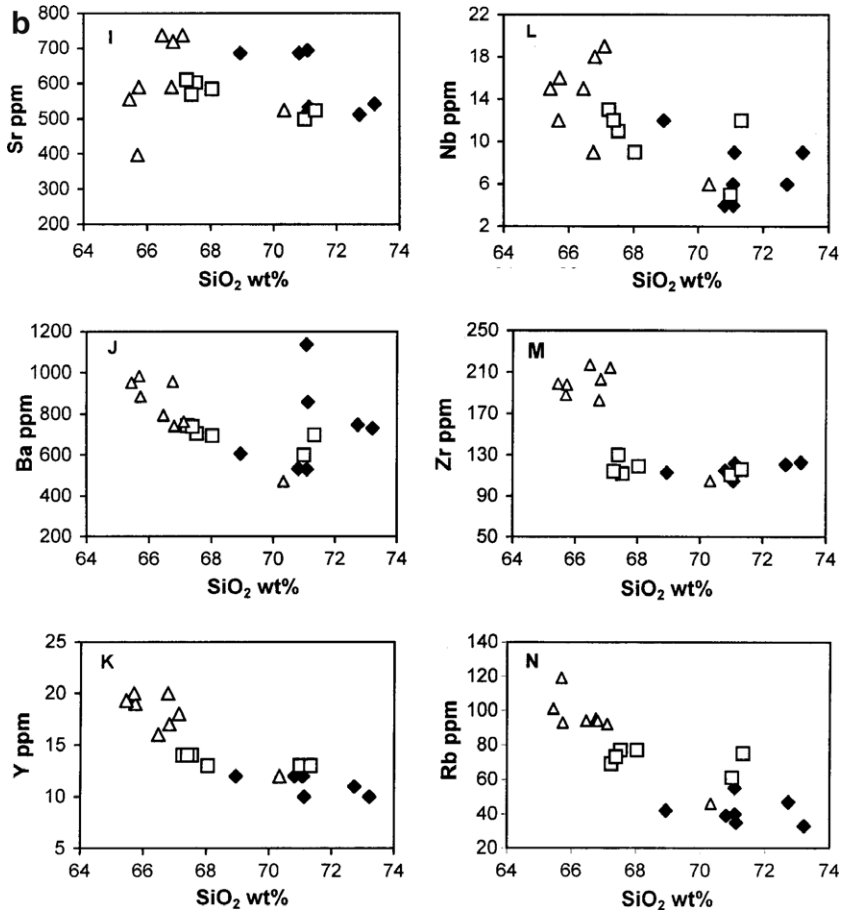

Fig. 8 (*continued*)

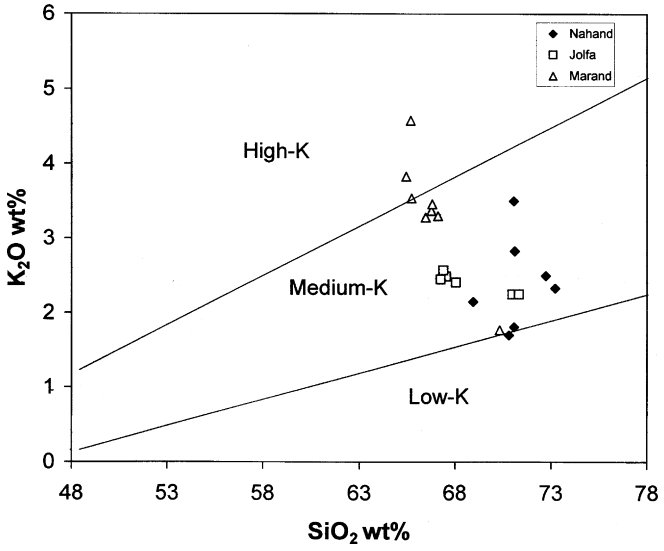

Fig. 9. SiO_2 vs. K_2O for dacitic rocks of NW Iran. Most of the samples plot in the medium-K field. High-K samples suspected of crustal contamination.

that small amounts of adakitic melt are entirely consumed in reaction with mantle peridotite to form metasomatized zones, as has been proposed by Sekine and Wyllie (1982) and Sen and Dunn (1995). On the other hand, when the ratio of melt/peridotite reaches 2:1, a portion of melt not consumed in the reaction becomes Mg-enriched and preserves its trace-element geochemical characteristics such as high Sr/Y and La/Yb ratios.

The highly enriched N-MORB normalized abundance patterns of trace elements and REE pattern for adakitic dacites and rhyodacites of NW Iran suggest the existence of garnet as a residue in the source. The enrichment of Sr and absence of negative Eu anomalies indicate that the residual source was plagioclase free. The Nb and Ti are strongly depleted in the studied samples, which suggest that the source also has residual rutile and amphibole and thus was most probably hydrous garnet-amphibolite or amphibole-eclogite. This garnet-bearing source implies that there are at least two possibilities for generation of adakitic rocks in NW Iran; partial melting of thickened lower crust and/or melting of subducted oceanic slab.

It is expected that crustal thickening caused by Arabian–Asian continental collision would result in transformation of basaltic lower crust into garnet-amphibolite or amphibole-eclogite. However, such deeper crustal materials have not been observed nor reported as xenoliths from the studied area. Moreover, geophysical investigations indicate that

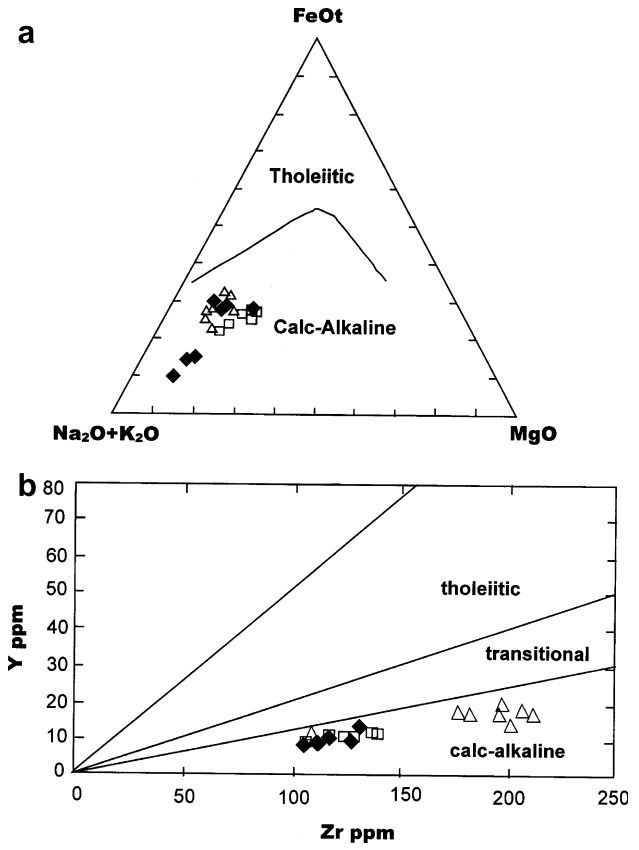

Fig. 10. (a) AFM diagram of Irvine and Baragar (1971) and (b) diagram of Y vs. Zr after MacLean and Barrett (1993) all samples plot in the calc-alkaline field.

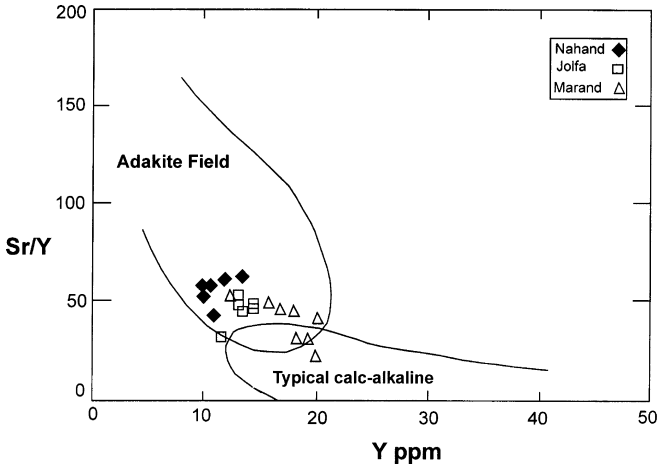

Fig. 11. Y vs. Sr/Y diagram (after Defant and Drummond, 1990) used to differentiate adakitic magmas from typical calc-alkaline magmas.

the thickness of crust in this area is about 40–45 km (Dehghani and Makris, 1984), which is not an adequate depth for conversion of basaltic lower crust into garnet-amphibolite or amphibole-eclogite.

The other candidate for hydrous amphibole-eclogite or garnet-amphibolite, which could melt to generate adakitic magmas in NW Iran, is subducted Neo-Tethyan oceanic slab. Controversy exists in the literature about the timing of the closure of Neo-Tethys along the Zagros suture. Some authors infer a Late Cretaceous age for continental collision (Berberian and King, 1981; Alavi, 1994). An alternative idea is that continental collision along the Zagros suture occurred in the Miocene (e.g., Berberian et al., 1982; Sengör et al., 1988; Sengör and Natal'in, 1996).

Paleoceanographic constraints derived from carbon and oxygen isotopic data indicate that Neo-Tethys had a connection with the northern Indian Ocean until 14 Ma (Woodruff and Savin, 1989). This factor supports the Miocene reconstruction of Neo-Tethys by Sengör and Natal'in (1996) and is independent of regional geological evidence. Existence of widespread shallow marine and limited deep-marine Paleocene to Miocene sediments in Zagros sub-zones is consistent with the south arm of the Tethys remaining open into the Miocene (Mohajjel et al., 2003). Opening of the Red Sea and the Gulf of Aden resulted in rotation of the Arabian plate with respect to Africa (Nubia and Somalia) since 30 Ma (Bonatti, 1987; Hempton, 1987; Guiraud and Bosworth, 1999). This plate movement was responsible for oblique convergence between the Arabian plate and central Iran and final closure of Neo-Tethys.

Petrological studies carried out in NW Iran and adjacent areas, i.e. to the east of Anatolia indicate that post-collisional magmas exhibit various geochemical enrichment signatures. The significant character of post-collisional magmatism in this area, progressive evolution of magmatic products from subalkalic to alkaline composition (Ahmadzadeh, 2002), and onset of post-collisional magmatism in the Late-Miocene in NW Iran with adakitic geochemical signatures, indicate the role of slab melting after cessation of subduction. The temporal and spatial relationship of the studied adakitic rocks with alkaline volcanic rocks may be attributed to slab roll-back and possibly break-off of subducted Neo-Tethyan oceanic lithosphere beneath the Central Iranian continental microplate. Slab break-off may have led to thermal perturbation resulting in melting of the detached slab and metasomatizm of the mantle in NW Iran and adjacent areas during the post-collisional event. Ascent of slab-derived magmas through thickened continental crust in this region could have been the cause of crustal contamination resulting in high Rb/Sr ratios and increase of K_2O, Th, and Y contents due to assimilation and fractional crystallization (AFC) processes. Evidence for AFC processes is marked by enrichment of K_2O over Na_2O or incompatible LILE enrichment such as Rb, Th, and Ba over HFSE like Zr (Esperanca et al., 1992, Fig. 15).

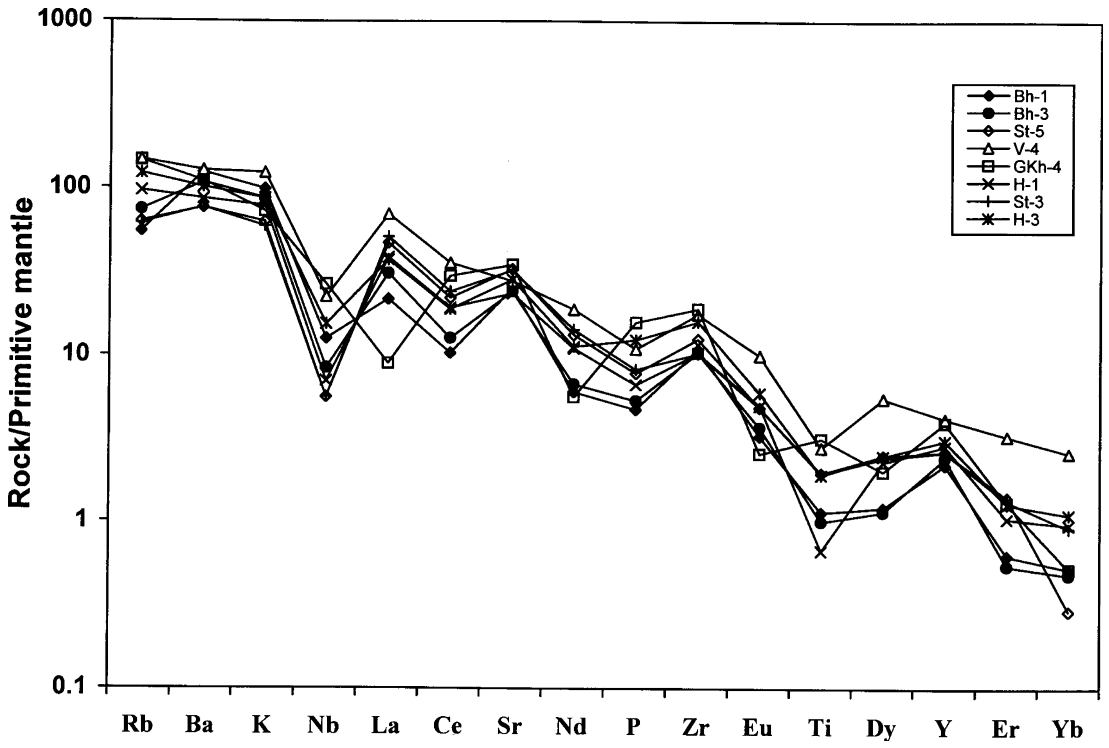

Fig. 12. Primitive mantle-normalized incompatible trace element diagram for selected samples. Normalizing data are from McDonough et al. (1992).

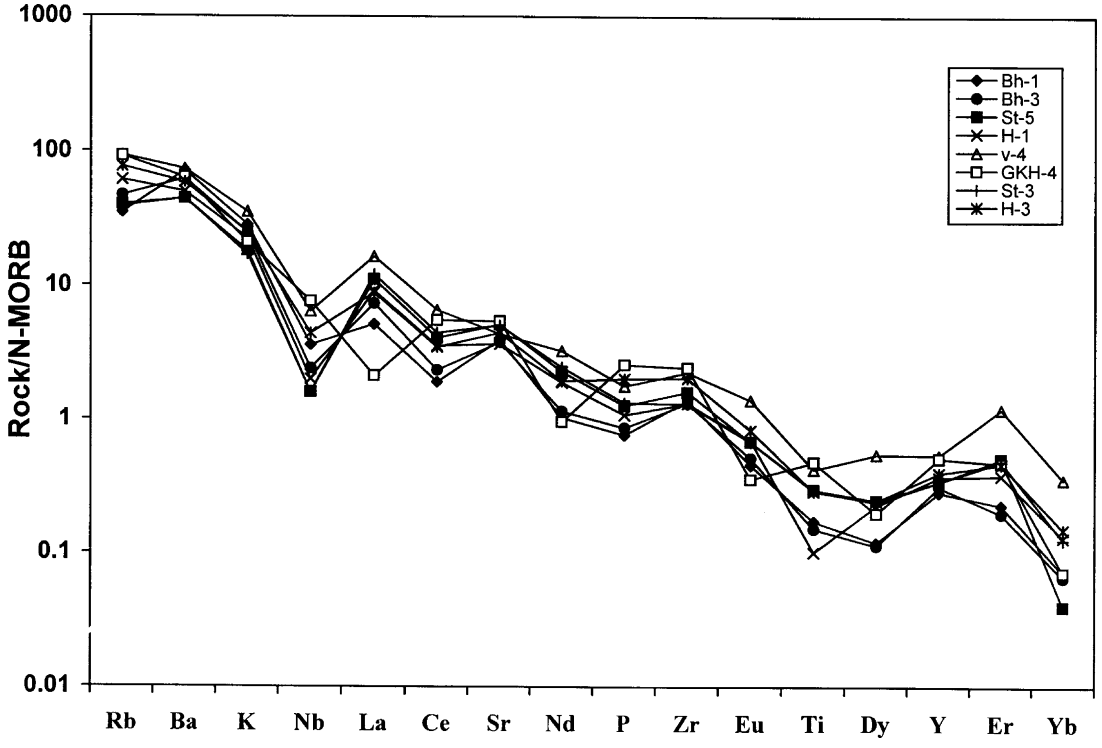

Fig. 13. MORB-normalized incompatible trace element diagram for selected representative samples. Normalizing data and the arrangement of incompatibility of elements from Pearce and Parkinson (1993).

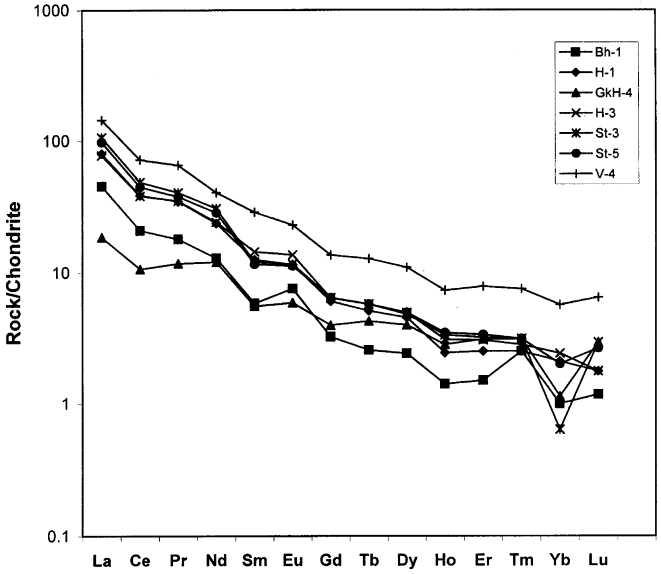

Fig. 14. Chondrite-normalized REE pattern of representative dacitic samples of NW Iran. Chondrite-normalizing data from Wakita et al. (1971).

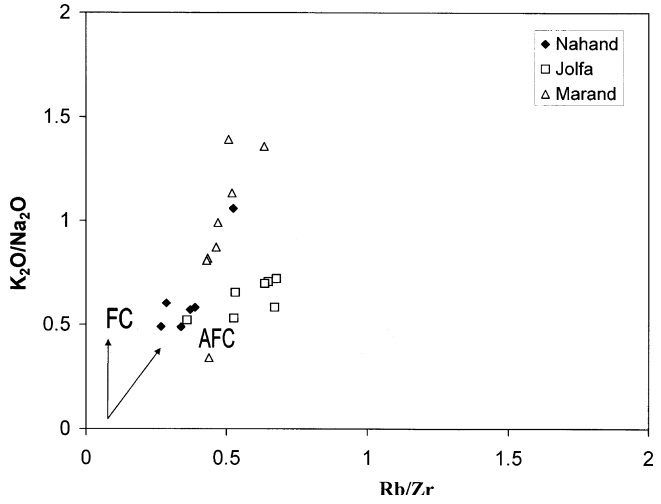

Fig. 15. Diagram of K_2O/Na_2O vs. Rb/Zr ratios shows fractional crystallization (FC) and assimilation fractional crystallization (AFC) trends.

6. Conclusions

(1) In NW Iran, numerous subvolcanic dacitic to rhyodacitic domes were intruded into different rocks during the Late Miocene. They exhibit porphyritic texture with phenocrysts of plagioclase and hornblende.
(2) The geochemical characteristics of subalkaline dacitic to rhyodacitic rocks include high LILE, LREE, Sr, strongly fractionated REE patterns and low content of HREE and Y showing similarities with adakites.
(3) The occurrence of adakitic rocks among the post-collisional magmatic rocks could represent the first magmatic products after cessation of Neo-Tethys subduction in the Urumieh-Dokhtar magmatic arc.
(4) The temporal and spatial association of adakitic rocks and alkaline volcanic rocks in the studied area can be attributed to slab break-off and melting of a detached slab and metsomatized mantle.
(5) Volcanism along the dextral strike-slip faults is mainly related to extension, followed by strike-slip tectonics in the context of regional tension.
(6) The variations in K_2O, LILE and HFSE contents in comparison with modern adakites can be attributed to assimilation, fractionation and crystallization processes.

Acknowledgements

This research is based on field and laboratory studies carried out at the University of Tabriz. Funding for this project was provided by Research office (No. 27/528) at the University of Tabriz and I wish to acknowledge the kind support of the staff of this office. Comments and constructive suggestions by D. Lentz and an anonymous reviewer are greatly appreciated. Deserved thanks go to M. Moayyed for his field assistance. N. Mosaiebzadeh is thanked for technical assistance and N. Ashrafi for reading the manuscript and his constructive comments.

References

Ahmadzadeh, G.R., 2002. Petrographical and Petrological Studies of Volcanic Rocks in NW of Marand (north of Galleban). Unpublished M.Sc. thesis, University of Tabriz, 114pp. (in Persian).
Alavi, M., 1994. Tectonics of the Zagros Orogenic belt of Iran: new data and interpretations. Tectonophysics 220, 211–238.
Alavi, M., 2004. Regional stratigraphy of the Zagros fold-thrust belt of Iran and its proforeland evolution. American Journal of Science 304, 1–20.
Amidi, S.M., Emami, M.H., Michel, R., 1984. Alkaline character of Eocene volcanism in the middle part of Iran and its geodynamic situation. Geologische Rundschau 73, 917–932.
Asadian, A., 1993. Geological map of Tabriz, 1:100000. Geological Survey of Iran.
Atherton, M.P., Petford, N., 1993. Generation of sodium-rich magmas from newly underplated basaltic crust. Nature 362, 144–146.
Berberian, F., Berberian, M., 1981. Tectono-plutonic episodes in Iran. In: Gupta, H.K., Delany, F.M. (Eds.), Zagros, Hindukosh, Himalaya. Geodynamic Evolution. American Geophysical Union, Washington, DC, pp. 5–32.
Berberian, M., King, G.C., 1981. Towards a paleogeography and tectonics evolution of Iran. Canadian Journal of Earth Sciences 18, 210–265.
Berberian, F., Muir, I.D., Pankhurst, R.J., Berberian, M., 1982. Late Cretaceous and early Miocene Andean type plutonic activity in northern Makran and central Iran. Journal of Geological Society of London 139, 605–614.
Bonatti, E., 1987. Oceanic evolution, rifting or drifting in the Red Sea. Nature 330, 692–693.
Chung, S.L., Chu, M.F., Zhang, Y., Xie, Y., Lo, C.H., Lee, T.Y., Ching-Ying Lan, C.Y., Xianhua Li, X., Zhang, O., Wang, Y., 2005. Tibetan

tectonic evolution inferred from spatial and temporal variations in post-collisional magmatism. Earth Sciences Review 68, 173–198.
Defant, M.J., Drummond, M.S., 1990. Derivation of some modern arc magmas by melting of young subducted lithosphere. Nature 34, 662–665.
Dehghani, G.A., Makris, T., 1984. The gravity field and crustal structure of Iran. Neues Jahrbuch für Geologie und Palaontologie-Abhandlungen 168 (2–3), 215–229.
Drummond, M.S., Defant, M.J., 1990. A model for trondhjemite-tonalite-dacite genesis and crustal growth via slab melting: Archaean to modern comparisons. Journal of Geophysical Research 95, 21503–21521.
Emami, H., 1981. Geologie de la reigon de Qom-Aran (Iran) contribution a l' etude denamique et geochemique du volcanisme Teriaire de l' Iran centaral. Unpublished Ph.D these, University Sc. Et Medical de Grenoble, 489 pp.
Esperanca, S., Crisci, M., de Rosa, R., Mazzuli, R., 1992. The role of the crust in the magmatic evolution of the island Lipari (Aeolian Islands, Italy). Contributions to Mineralogy and Petrology 112, 450–462.
Farhoudi, G., 1978. A comparison of Zagros geology to island arcs. Journal of Geology 86, 323–334.
Förster, H., Fesefeldt, K., Kursten, M., 1972. Magmatic and orogenic evolution of the Central Iranian volcanic belt. In: 24th International Geology Congress, Section 2, pp. 198–210.
Ghasemi, A., Talbot, C.J., 2006. A new tectonic scenario for the Sanandaj-Sirjan Zone (Iran). Journal of Asian Earth Sciences 26, 683–693.
Guiraud, R., Bosworth, W., 1999. Phanerozoic geodynamic evolution of northeastern Africa and northwestern Arabian platform. Tectonophysics 282, 39–82.
Hassanzadeh, J., 1993. Metallogenic and tectonomagmatic events in the SE sector of the Cenozoic active continental margin of Iran (Shahre-Babak area, Kerman Province). Unpublished Ph.D thesis, University of California, Los Angeles, 204pp.
Hempton, M.R., 1987. Constraints on Arabian plate motion and extensional history of the Red Sea. Tectonics 6, 687–705.
Irvine, T.N., Baragar, W.R.A., 1971. A guide to the chemical classification of the common volcanic rocks. Canadian Journal of Earth Sciences 8, 523–548.
Jung, D., Kursten, M., Tarkian, M., 1976. Post-Mesozoic volcanism in Iran and its relation to the subduction of the Afro-Arabian under the Eurasian plate. In: Pilger, A., Rosler, A. (Eds.), A far Between Continental and Oceanic Rifting. Schweizerbartsche Verlagbuchhandlung, Stuttgart, pp. 175–181.
Karapetian, S.G., Jrbashian, R.T., Mnatsakanian, A.Kh., 2001. Late collision rhyolitic volcanism in the north-eastern part of the Armenia Highland. Journal of Volcanology and Geothermal Research 12, 189–220.
Karimzadeh Somarin, A., 2004. Marano volcanic rocks, East Azerbaijan Province, Iran, and associated Fe mineralization. Journal of Asian Earth Sciences 24, 11–23.
Kay, R.W.J., 1978. Aleutian magnesian andesites: melts from subducted Pacific oceanic crust. Journal of Volcanology and Geothermal Research 4, 117–132.
Le Maitre, R.W., Bateman, P., Dudek, A., Keller, J., Le Bas, M.J., Sabine, P.A., Schmid, R., Sorensen, H., Streckeisen, A., Woolley, A.R., Zanettin, B., 1989. A Classification of Igneous Rocks and Glossary of Terms. Blackwell, Oxford, 193 pp.
Martin, H., 1993. The mechanisms of petrogenesis of the Archaean continental crust, comparison with modern processes. Lithos 30, 373–388.
Martin, H., 1999. The adakitic magmas: modern analogues of Archaean granitoids. Lithos 46 (3), 411–429.
Maury, R.C., Sajona, F., Pubellier, M., Bellon, H., Defant, M., 1996. Fusion de la croute oceanique dans les zones de subdction/collision recentes: l' example de Mindanao (Philippines). Bulletin de la Societe Geologique de France 167, 579–595.
MacLean, W.H., Barrett, T.J., 1993. Lithochemical techniques using immobile elements. Journal of Geochemical Exploration 48, 109–133.
McDonough, W.F., Sun, S., Ringwood, A.F., Jagoutz, E., Hofmann, A.W., 1992. Rb and Cs in the earth and moon and evolution of the earth's mantle. Geochimica et Cosmochimica Acta 56 (3), 1001–1012.
Mohajjel, M., Fergusson, C.L., Sahandi, M.R., 2003. Cretaceous-Tertiary convergence and continental collision, Sanandaj-Sirjan Zone, western Iran. Journal of Asian Earth Sciences 21, 397–412.
Moradian, A., 1997. Geochemistry, Geochronology and Petrography of Feldspathoid Bearing Rocks in Urumieh-Dokhtar Volcanic Belt, Iran. Unpublished Ph.D thesis, University of Wollongong, Australia, 412pp.
Peacock, S.M., Rushmer, T., Thompson, A.B., 1994. Partial melting of subducting oceanic crust. Earth and Planetary Science Letters 121, 224–227.
Pearce, J.A., Parkinson, I.J., 1993. Trace element models for mantle melting: application to volcanic arc petrogenesis. In: Prichard, H.M., Alabaster, T., Harris, N.B.W., Neary, C.R. (Eds.), Magmatic Processes in Plate Tectonics, vol. 76. Geological Society of London Special Publication, pp. 373–403.
Pe-Piper, G., Piper, D.W.J., 1994. Miocene magnesian andesites and dacites, Evia, Greece: adakites associated with subducting slab detachment and extension. Lithos 31, 125–140.
Petford, N., Atherton, M.P., 1996. Na-rich partial melts from newly underplated basaltic crust, Cordillera Blanca batholith, Peru. Journal of Petrology 37, 1491–1521.
Prouteau, G., Maury, R.C., Rangin, C., Suparka, E., Bellon, H., Pubellier, M., Cotten, J., 1996. Les adakites miocenes du NW Borneo, temoins de la fermeture de la proto-mer de Chine. C.R. Acad. Sci. Paris 323 serie IIa, pp. 925–932.
Rapp, R.P., Watson, E.B., Miller, C.F., 1991. Partial melting of amphibolite/eclogite and the origin of Archaean trondhjemites and tonalites. Precambrian Research 51, 1–25.
Rapp, R.P., Shimizu, N., Norman, M.D., Applegate, G.S., 1999. Reaction between slab-derived melts and peridotite in the mantle wedge: experimental constraints at 3.8 GPa. Chemical Geology 160, 335–356.
Reagan, M.K., Gill, J.B., 1989. Coexisting calc-alkaline and high niobium basalts from Turrialba volcano, Costa Rica: implications for residual titanates in arc magma sources. Journal of Geophysical Research 94, 4619–4633.
Ricou, L.E., 1994. Tethys reconstruction: plates, continental fragments and their boundaries since 260 Ma from Central America to South-eastern Asia. Geodinamica Acta (Paris) 7 (4), 169–218.
Sadeghzadeh, M., 2004. Structural Investigations on the North-Misho Fault. Unpublished M.Sc thesis, University of Tabriz, Iran, 103pp. (in Persian).
Sajona, F.G., Maury, R.C., Bellon, H., Cotten, J., Defant, M.J., Pubellier, M., Rangin, C., 1993. Initiation of subduction and the generation of slab melts in western and eastern Mindanao, Philippines. Geology 21, 1007–1010.
Sajona, F.G., Bellon, H., Maury, R.C., Pubellier, M., Cotten, J., Rangin, C., 1994. Magmatic response to abrupt changes in tectonic setting: Pliocene-Quaternary calc-alkaline lavas and Nb-enriched basalts of Leyte and Mindanao Philippines. Tectonophysics 237, 47–72.
Sajona, F.G., Maury, R.C., Pubellier, M., Letirrier, J., Bellon, H., Cotten, J., 2000. Magmatic source enrichment by slab-derived melts in a young post-collision setting, Central Mindanao (Philippines). Lithos 54, 173–206.
Seghedi, I., Downes, H., Vaselli, O., Szakacs, A., Balogh, K., Pecskay, Z., 2004. Post-collisional Tertiary-Quaternary mafic alkalic magmatism in the Carpathian-Pannonian region: a review. Lithos 72, 117–146.
Sekine, T., Wyllie, P.J., 1982. Experimental simulation of mantle hybridization in subduction zones. Journal of Geology 91, 511–528.
Sen, C., Dunn, T., 1994. Dehydration melting of a basaltic composition amphibolite at 1.5 and 2.0 GPa: implications for the origin of adakites. Contributions to Mineralogy and Petrology 117, 394–409.
Sen, C., Dunn, T., 1995. Experimental modal metasomatism of a spinel lherzolite and the production of amphibole-bearing peridotite. Contributions to Mineralogy and Petrology 119, 422–432.

Sengör, A.M.C., 1984. The Cimmeride Orogenic System and the Tectonics of Eurasia. Geological Society of America Special Paper, 195pp.

Sengör, A.M.C., Natal'in, B.A., 1996. Paleotectonic of Asia: fragments of a synthesis. In: Yin, A., Harrison, T.M. (Eds.), The Tectonic Evolution of Asia. Cambridge University Press, Cambridge, pp. 486–640.

Sengör, A.M.C., Altmer, D., Cin, A., Ustaomer, T., Hsu, K.J., 1988. Origin and assemble of the Tethyside orogenic collage at the expense of Gondwanaland. In: Audley-Charls, M.G., Hallam, A. (Eds.), Gondwana and Tethys. Geological Society of London, Special Publication, 37, pp. 19–181.

Stöcklin, J., 1972. Iran central, septentrional et oriental. Lexique stratigraphique international, III, Fasicule 9b, Iran, Centre National de la Recheche Scientifique, Paris, pp. 1–283.

Stöcklin, J., 1974. Possible ancient continental margins in Iran. In: Burk, C.A., Drake, C.L. (Eds.), The Geology of Continental Margins. Springer, Berlin, pp. 873–887.

Wakita, H., Rey, P., Schmitt, R.A., 1971. Abundances of the 14 rare earth elements and 12 other trace elements in Apollo 12 samples: five igneous and one breccia rocks and four soils. In: Proceedings of the Second Lunar Science Conference. Pergamon Press, Oxford, pp. 1319–1329.

Wilson, M., 1989. Igneous Petrogenesis: A Global Tectonic Approach. Harper Collins Academic, 466 p.

Winchester, J.A., Floyd, P.A., 1977. Geochemical discrimination of immobile elements. Chemical Geology 20, 325–343.

Woodruff, F., Savin, S.M., 1989. Miocene deep water oceanography. Paleoceanography 4, 87–140.

Yogodzinski, G.M., Kay, R.W., Volynets, O.N., Koloskov, A.V., Kay, S.M., 1995. Magnesian andesite in the western Aleutian Komandorsky region: implications for slab melting and processes in the mantle wedge. Geological Society of America Bulletin 107 (5), 505–519.